CHEMISTRY OF MATERIALS

ARTICLE

pubs.acs.org/cm

New Sulfonated Poly(*p*-phenylenesulfone)/Poly(1-oxotrimethylene) Nanocomposite Proton-Conducting Membranes for PEMFCs

Vito Di Noto,*[,†] Matteo Piga,[†] Guinevere A. Giffin,[†] Michael Schuster,[‡] Gianni Cavinato,[†] Luigi Toniolo,[§] and Stefano Polizzi[∥]

[†]Department of Chemical Sciences, University of Padova, Via Marzolo 1, I-35131, Padova (PD), Italy

[‡]Fuma-Tech GmbH, Steinbeisstrasse 41-43, D-71665 Vaihingen/Enz, Germany

[§]Department of Chemistry, Università Ca' Foscari di Venezia, Dorsoduro, Calle Larga S. Marta 2137, 30123 Venezia, Italy

[∥]Department of Physical Chemistry, Università Ca' Foscari di Venezia, Via Torino 155/B, I-30123 Venezia-Mestre, Italy

ABSTRACT: Two series of membranes, A and B, were prepared by the following synthesis protocols. A-type membranes were obtained by a solvent casting process from solutions prepared by dissolving three different blends of poly(1-oxotrimethylene) (PK) and sulfonated poly(*p*-phenylenesulfone) ($sPSO_2$) in DMAc. B-type materials were prepared using a two-step process. First, an inorganic−organic hybrid nanofiller was synthesized by CO-ethene copolymerization in the presence of silica nanoparticles. From this synthesis, a hybrid nanofiller, $[SiO_2/(PK)_{0.65}]$, with 35 wt % of SiO_2 was obtained. Membranes were produced by a solvent casting process from solutions prepared by dispersing different amounts (10, 20, 30 wt %) of the $[SiO_2/(PK)_{0.65}]$ nanofiller in a $sPSO_2$/DMAc solution. As compared to pristine $sPSO_2$ and the A-type materials, the presence of the hybrid nanofiller in the B-type membranes reduces the water uptake and membranes' swelling and increases the proton conductivity at low membrane hydration levels.

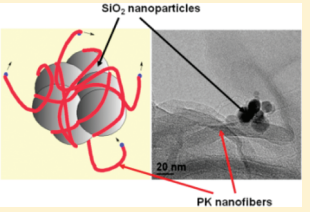

KEYWORDS: hybrid inorganic−organic membranes, polysulfone, polyketone, silica, proton exchange membrane fuel cell, dynamic mechanical analysis, proton conductivity

1. INTRODUCTION

One of the main targets in the academic and industrial research of proton exchange membrane fuel cells (PEMFCs) is the development of new proton-conducting membranes capable of operating at temperatures higher than 90 °C and at low relative humidity.[1,2] Despite their high cost perfluorinated ionomers, such as Dupont's Nafion, are the most widely studied and applied materials.[3,4] They function very well up to ca. 90 °C at high relative humidity.[5] However at temperatures greater than 90 °C, they are characterized by a poor performance owing to the membrane dehydration processes and the bulk thermo-mechanic transitions.[6]

A number of poly(arylene)-based ionomers such as sulfonated poly(ether ether ketone) or poly(ethersulfone) have been proposed,[7−10] which present lower methanol crossover and improved mechanical characteristics at temperatures above 90 °C as compared to the classical perfluorosulfonic acid polymers. In poly(arylene)-based ionomers, a reasonable ionic conductivity for practical applications in PEMFCs is obtained when a proton exchange capacity higher than two mequiv•g^{-1} is reached.[11] Nevertheless, under the hydration conditions typically adopted in PEMFCs, such a high proton exchange capacity leads to swelling and the loss of the membranes' mechanical properties. These effects result in decreased membrane performance in PEMFCs and in many cases dissolution in water above 50 °C.[10] Other poly(arylene) ionomers, such as sulfonated poly(*p*-phenylenesulfone), characterized by electron-deficient poly(arylene) chains and high ionic exchange capacity (IEC) were proposed.[11−13] The first property acts to increase the acidity and the thermal and thermo-oxidative stability of the materials, while the latter is a crucial parameter in improving the proton conductivity. Sulfonated poly(*p*-phenylenesulfone) presents lower solubility and swelling in water and improved chemical stability[11−13] as compared to other sulfonated poly(arylene)s with similar IECs. These properties are nevertheless insufficient for practical application in PEMFCs operating at high temperatures. In this study, nanocomposite proton-conducting membranes were prepared with the aim of stabilizing sulfonated poly(*p*-phenylenesulfone) ($sPSO_2$) with an equivalent weight (EW) of 360 g•equiv^{-1}. The low EW, which corresponds to a high IEC of 2.77 mequiv•g^{-1} and a degree of sulfonation equal to 50%, is the reason for the large variation in mechanical properties with relative humidity. Under dry conditions $sPSO_2$ is very hard and brittle, but as the relative humidity increases, it starts to swell and loses its integrity at high water activities.[11−13]

This work describes the preparation of new $sPSO_2$-based nanocomposite membranes with very low swelling and good electrical and mechanical properties above 70 °C. The materials were obtained by modulating the properties of $sPSO_2$ with poly(1-oxotrimethylene) (PK). The polyketone copolymer was obtained by alternating CO-ethene copolymerization.[14,15] This strategy is very innovative and promising. It allows the enhancement of the thermal and mechanical properties of

Received: May 26, 2011
Revised: September 13, 2011
Published: September 30, 2011

dx.doi.org/10.1021/cm2014797 | *Chem. Mater.* 2011, 23, 4452–4458

nanocomposite $sPSO_2$ membranes, making them suitable for application in PEMFCs. PK is a copolymer that is very stable both chemically and thermally.[14,15] Two series of membranes, A and B, were prepared. Both types of membranes were obtained by a two-step process. For the A-type materials 1) different copolymerization times for the reaction of CO with ethene in the presence of $sPSO_2$ were used to obtain a PK/$sPSO_2$ blend with 11, 28, and 33 wt % of PK; and 2) membranes were prepared by a solvent casting process from solutions containing the three different PK/$sPSO_2$ blends dissolved in dimethylacetamide (DMAc). For the B-type materials 1) an inorganic−organic hybrid nanofiller $[SiO_2/(PK)_{0.65}]$, where the weight fraction of PK equals 0.65, was synthesized by CO-ethene copolymerization in the presence of silica nanoparticles; and 2) a solvent casting process was used to prepare membranes by dispersing 10, 20, 30 wt % of $[SiO_2/(PK)_{0.65}]$ nanofiller in a $sPSO_2$/DMAc solution. The mechanical properties and the relaxation processes were investigated by dynamical mechanical analyses (DMA), revealing the presence of three mechanical transitions, α, β, and γ. The electrical properties were studied by broadband electric spectroscopy (BES). Electrical measurements were conducted for fully hydrated samples and at different values of relative humidity, in order to elucidate the effect of the inorganic nanofiller on the proton conduction as a function of the membranes' hydration state.

Results indicate that the presence of the hybrid nanofiller in B-type membranes reduces the water uptake and membrane swelling and increases the proton conductivity at low levels of membrane hydration as compared to pristine $sPSO_2$ and A-type materials.

2. EXPERIMENTAL SECTION

2.1. Preparation of Materials by CO/Ethene Copolymerization. $[SiO_2/(PK)_{0.65}]$, where the weight fraction (weight of polyketone/total weight) is 0.65, was prepared by CO-ethene copolymerization in the presence of porous silica by the following procedure. 8.8 mg (0.01 mmol) of $[Pd(TsO)(H_2O)(dppp)](TsO)\cdot H_2O$,[16] 19 mg (0.1 mmol) of $TsOH\cdot H_2O$, ca. 1.3 g of porous silica, and 80 mL of MeOH were added to a glass bottle and placed in an autoclave (dppp = 1,3-bis(diphenylphosphino)propane; TsO = 4-methylbenzene sulfonate). The autoclave was flushed with CO, pressurized to 45 atm with CO/ethene (1:1 ratio), and heated at 85 °C. The autoclave was maintained at this temperature for 1 h and then cooled to room temperature and depressurized. The sample was constantly stirred during the reaction process. The resulting solid was collected by filtration, washed with MeOH, and dried under vacuum to yield 3.430 g of $[SiO_2/(PK)_{0.65}]$. A similar procedure was followed for the preparation of the fillers $[sPSO_2/(PK)_{0.11}]$, $[sPSO_2/(PK)_{0.28}]$ and $[sPSO_2/(PK)_{0.33}]$ used in the preparation of the A-type membranes, except that $sPSO_2$ was added in place of silica and the reaction times varied from 3 to 8 h.

2.2. Preparation of the Membranes. Pristine $sPSO_2$ membrane, used as reference material, was prepared by dissolving 500 mg of sulfonated poly(*p*-phenylenesulfone) (EW = 360 g·equiv^{-1}) in 7 mL of DMAc. The solution was recast onto a Petri dish and maintained at 80 °C and under a dry air flow. The film was peeled from the Petri dish in 2-propanol and cured at 190 °C for 15 h. The same procedure was followed for the preparation of A-type membranes, except that $[sPSO_2/(PK)_x]$, with x = 11, 28, and 33 wt % was used instead of pristine $sPSO_2$. B-type membranes, having a composition of $[sPSO_2/(SiO_2)_y\cdot(PK)_z]$, where y and z are the respective weight fractions of SiO_2 and PK, were prepared by dissolving $sPSO_2$ in DMAc and by adding 10, 20, and 30 wt % of $[SiO_2/(PK)_{0.65}]$ filler to the solution. The dispersions were homogenized by sonication and then recast onto a Petri dish as above. The resulting membranes are labeled $[sPSO_2/(SiO_2)_{0.035}(PK)_{0.065}]$, $[sPSO_2/(SiO_2)_{0.069}(PK)_{0.131}]$, and $[sPSO_2/(SiO_2)_{0.104}(PK)_{0.196}]$ indicating membranes containing 10, 20, and 30 wt % of hybrid filler, respectively.

2.3. Instruments and Methods. The proton exchange capacity was determined as follows. About 100 mg of each sample was dried for one week over P_2O_5, weighed in inert atmosphere, soaked in 100 mL of KCl 1 M, and left stirring overnight. The solution was then titrated with 0.01 M KOH using a phenolphthalein indicator.

The water uptake (W.U.) and the number of water molecules per sulfonic acid group (λ) were determined by TGA measurements as described elsewhere[17] after soaking the samples in water at room temperature for one day. The initial (wt_0) and dry (wt_{dry}) weight of each sample was determined by registering the isothermal TGA desorption profile at 30 °C. The W.U. was determined using the following equation

$$\text{W.U.} = \frac{wt_0 - wt_{dry}}{wt_{dry}} \quad (1)$$

λ depends on the W.U. and on the Ionic Exchange Capacity (IEC) as follows[18,19]

$$\lambda = 1000\left[\frac{\text{W.U.}}{MW_{H_2O}\text{IEC}\chi_{sPSO_2}}\right] \quad (2)$$

where MW_{H2O} is the molecular weight of water, and χ_{sPSO_2} is the weight fraction of $sPSO_2$.

High-resolution transmission electron microscopy (HR-TEM) images were collected using a Jeol 3010 instrument operating at 300 kV with a high resolution pole piece (0.17 nm point-to-point resolution) and equipped with a Gatan slow-scan 794 CCD camera.

The infrared spectra of pristine PK, SiO_2, and $[SiO_2/(PK)_{0.65}]$ powders were collected using a Nicolet FT-IR Nexus spectrometer equipped with a Smart Diffuse Reflectance Accessory (Thermo Scientific).

Dynamic mechanical analyses (DMA) were carried out with a DMA Q800 (TA Instruments) using the film/fiber tension clamp. Temperature spectra were measured by subjecting a rectangular sample to an oscillatory sinusoidal tensile deformation at 1 Hz with an amplitude of 4 μm and a preloading force of 0.05 N. Measurements were carried out in the range of temperature from −100 to 250 °C at a rate of 4 °C·min^{-1}. Before the measurements, each sample was dried at room temperature overnight. The mechanical response of the materials was analyzed in terms of elastic (E′), storage modulus (E″), and tan δ = E″/E′.

The measurement of the complex conductivity spectra of wet samples was carried out in the frequency range from 10 mHz to 10 MHz using a Novocontrol Alpha-A analyzer. The temperature range from 5 to 155 °C was explored using a homemade cryostat operated with a N_2 gas jet heating and cooling system. The measurements were performed in a closed homemade cell that allowed the water to be retained in the wet membrane in the explored temperature range. The geometric constant of the cell was determined by measuring the electrode−electrolyte contact surface and the distance between electrodes with a micrometer. The temperature was measured with accuracy greater than ±0.1 °C. Weighing the closed cell before and after the measurements ensured an absence of water loss. The complex impedance ($Z^*(\omega)$) was converted into complex conductivity ($\sigma^*(\omega) = \sigma'(\omega) + i\sigma''(\omega)$) using the equation

$$\sigma^*(\omega) = k\cdot[Z^*(\omega)]^{-1} \quad (3)$$

where k is the cell constant in cm^{-1}, and $\omega = 2\pi f$ (f is the frequency in Hz). The bulk conductivity of the samples, σ_0, was determined from the conductivity value extrapolated from the plateau of the $\sigma'(\omega)$ profiles at frequencies higher than 10^5 Hz, as described elsewhere.[20]

dx.doi.org/10.1021/cm2014797 |Chem. Mater. 2011, 23, 4452–4458

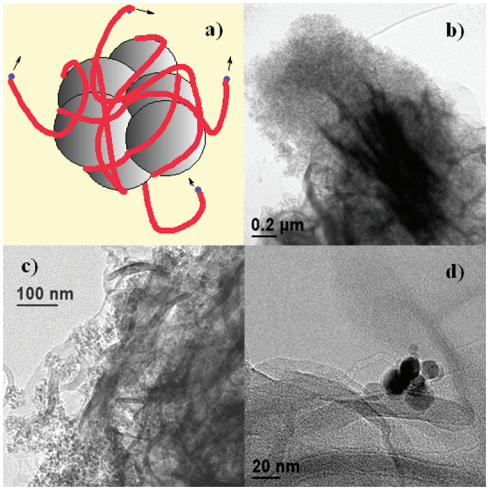

Figure 1. (a) Morphological hypothesis of the growth mechanism of PK on the surface of silica nanoparticle aggregates; (b) and (c) TEM images of the PK fibers wrapping the silica nanoparticle aggregates; (d) micrograph of primary silica nanoparticles wrapped with PK.

Electrical measurements at different relative humidity values were performed in the frequency range between 40 and 10^7 Hz using an Agilent 4294A Analyzer. The sample was placed between two steel porous electrodes inside a homemade chamber where the humidity is generated by an Arbin Instrument (USA) humidifier.[21] The relative humidity (R.H.), the Dew Point temperature (T_{DP}), and the temperature (T_C) inside the measuring chamber were controlled by an optical system (Optidew Remote, Michell Instruments) and a Pt100 sensor.[21]

3. RESULTS AND DISCUSSION

3.1. Hybrid Nanofiller Morphology. The morphology of the hybrid nanofiller was determined by HR-TEM (Figure 1). The results lead to crucial insights into the growth mechanism of the PK nanofibers on the surface of SiO_2, which are shown in Figure 1a. Figure 1b,c reveals that PK horse-hair nanofibers are wrapped around a granular mass core of silica nanoparticles, while the analysis of Figure 1d shows that the silica nanoparticles are about 20 nm in size.

The infrared spectra of SiO_2, $[SiO_2/(PK)_{0.65}]$ and the PK powders are reported in Figure 2. The infrared spectrum of the $[SiO_2/(PK)_{0.65}]$ hybrid nanofiller is essentially the superposition of SiO_2 and PK spectra. Furthermore, the presence of the OH stretching modes of hydroxyl groups in the spectra of both pristine SiO_2 and $[SiO_2/(PK)_{0.65}]$ between 3800 and 3000 cm^{-1} indicates that PK is coiled around the silica nanoparticles without forming chemical bonds with the OH groups present on the surface of the nanoparticles.

3.2. Water Uptake and Mechanical Properties. The composition and select properties of the materials explored in this study are reported in Table 1. For the sake of completeness, the properties of the A- and B-type membranes are compared with those of a pristine $sPSO_2$ reference membrane measured in the same conditions. The W.U. values are significantly different for each type of material studied (Table 1), while the number of water molecules per sulfonic acid groups (λ) is approximately the same for all membranes ranging between 7 and 11 except in the membranes with the highest amount of hybrid nanofiller (λ = 15). The W.U. of the A and B-type membranes is close to half of that of pristine $sPSO_2$, with the lowest W.U. occurring in the

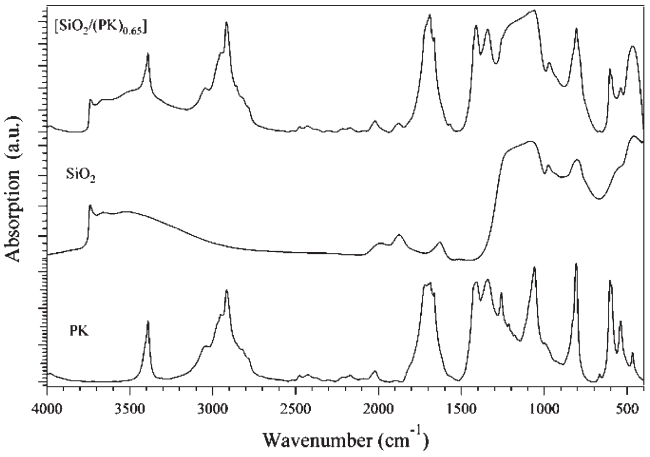

Figure 2. Infrared spectra of pristine PK, SiO_2 and the $[SiO_2/(PK)_{0.65}]$ hybrid nanofiller in the spectral region from 4000 to 400 cm^{-1}.

$[sPSO_2/(PK)_{0.33}]$ membrane. This effect is ascribed to the dilution of the hydrophilic acid groups of $sPSO_2$ by PK nanofiller in the bulk membranes that reduces the volume of the hydrophilic domains. Even if the weight fraction of $sPSO_2$ in the A and B groups is similar (Table 1), the water uptake for B-type membranes is higher than those measured for the A-type membranes. This is due to the high nanoporosity of the hybrid $[SiO_2/(PK)_{0.65}]$ nanofiller that absorbs water molecules in the interstices between the surface of silica nanoparticles and the wrapping PK nanofibers. Specifically, in agreement with the swelling percentage, S(%), reported in Table 1, it is observed that a) pristine polysulfone exhibits severe swelling even at room temperature and dissolves completely in boiling water; b) B-type membranes have a higher dimensional stability than $sPSO_2$ and only partially dissolve in boiling water; and c) A-type membranes exhibit no swelling at room temperature and are very stable even in boiling water. Polysulfone-based materials[22] have previously shown that the through-plane swelling is larger than the in-plane swelling. However, in this work the measuring equipment was not sufficiently precise to accurately determine the in-plane swelling, so only the through-plane is reported. These experimental results imply a decrease in permittivity and an improvement in mechanical stability of the nanocomposite membranes in polar environments such as water.

The mechanical properties of the dry materials were studied by DMA between −100 and 250 °C at 1 Hz. The profiles of the Storage Modulus (E′), the Loss Modulus (E″), and tan δ are shown in parts a) and b) of Figure 3 for A- and B-type membranes, respectively.

It is observed that up to ca. 200 °C, pristine dry $sPSO_2$ has a Storage Modulus (E′) higher than 1700 MPa (Figure 3). The mechanical properties of poly(*p*-phenylenesulfone) are much better than those of pristine Nafion, whose E′ values decrease steadily above 100 °C up to an irreversible elongation above 130 °C.[17−19,23,24] The E′ values of A-type membranes are lower than those of pristine $sPSO_2$ and the B-type materials, indicating that the density of hydrogen bonding cross-links in A-type membranes is lower than that in B-type. The difference in the mechanical properties of the A- and B-type membranes is due to the presence of the SiO_2 nanoparticles, which interact with the $sPSO_2$ acid groups to increase the mechanical stability of the hybrid membranes. In particular at temperatures above 100 °C,

dx.doi.org/10.1021/cm2014797 |*Chem. Mater.* 2011, 23, 4452–4458

Table 1. Composition, Ionic Exchange Capacity (IEC), Water Uptake (W.U.), Arrhenius and VTF Pseudo-Activation Energies of $sPSO_2$, and A- and B-Type Membranes[f]

	material	χ_{sPSO2}[a]	f[b]	IEC (meq·g^{-1})	W.U. (%)[c]	λ[c]	S(%)[d]	E_a (kJ·mol^{-1})[e] I	E_a (kJ·mol^{-1})[e] II
	$sPSO_2$	1	0	2.44	50	11	109	17	0.6
A Type	$[sPSO_2/(PK)_{0.11}]$	0.89	0.12	2.17	24	7	20	9	1.5
	$[sPSO_2/(PK)_{0.28}]$	0.72	0.38	1.76	25	11	22	23	2.8
	$[sPSO_2/(PK)_{0.33}]$	0.67	0.49	1.63	17	9	21	12	3.2
B Type	$[sPSO_2/(SiO_2)_{0.035}(PK)_{0.065}]$	0.90	0.07	2.20	31	9	30	19	1.2
	$[sPSO_2/(SiO_2)_{0.069}(PK)_{0.131}]$	0.80	0.16	2.00	29	10	24	16	1.4
	$[sPSO_2/(SiO_2)_{0.104}(PK)_{0.196}]$	0.70	0.28	1.70	33	15	22	13	1.3

[a] Weight fraction of poly(*p*-phenylene sulfone). [b] $f = (wt_{PK})/(wt_{sPSO_2})$. [c] Determined after soaking the sample one day in water at room temperature. [d] Percentage of swelling as compared to the dry membrane with the same treatment; $S(\%) = ((L\text{-}L_0)/L_0)\cdot 100$, where L_0 and L are the thickness of the dry and wet membrane, respectively. [e] Activation energies are determined from fitting the conductivity profiles of wet samples with Arrhenius (region I) and VTF (region II) equations. [f] λ is the ratio of water molecules per sulfonic acid group. I and II are the conductivity regions.

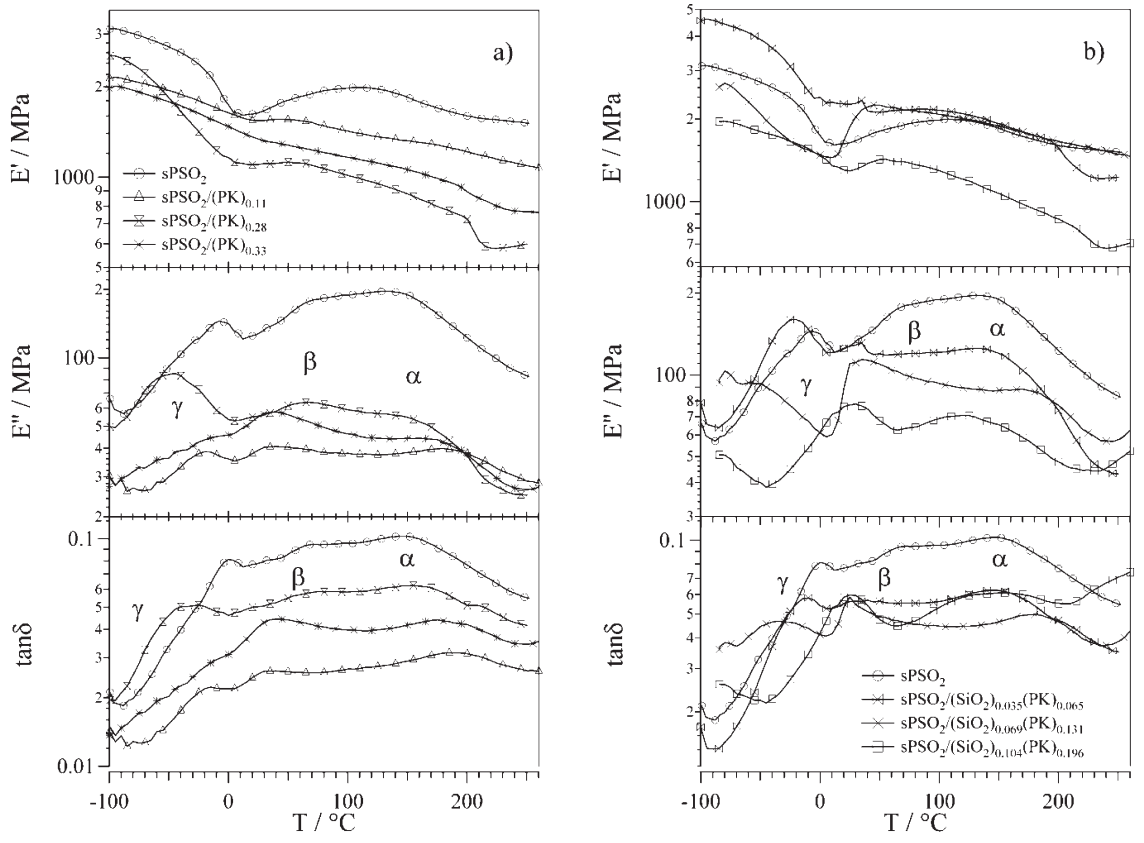

Figure 3. Profiles of the storage modulus (E′), loss modulus (E″), and tan δ = E″/E′ versus temperature of the dry membranes: a) $sPSO_2$ and A-type membranes and (b) $sPSO_2$ and B-type membranes.

the E′ values of membranes doped with 10 and 20 wt % of $[SiO_2/(PK)_{0.65}]$ nanofiller are similar to that of pristine $sPSO_2$, with values of 1980, 2088, and 2003 MPa at 120 °C for $sPSO_2$, $[sPSO_2/(SiO_2)_{0.035}(PK)_{0.065}]$ and $[sPSO_2/(SiO_2)_{0.069}(PK)_{0.131}]$, respectively. This indicates that at medium-high temperature, i.e. above 100 °C, the strength of the hydrogen bonding interactions between sulfonic acid groups of $sPSO_2$ are similar to those between $sPSO_2$ and the silica hydroxyl groups. The major drawback of $sPSO_2$ is that its mechanical properties are strongly influenced by its hydration state.[12,13] To reveal the effect of hydration on the mechanical properties, the A- and B-type membranes, which showed the best mechanical properties in a dry state were measured in a wet state at room temperature. Wet $sPSO_2$ has an E′ value of 16 MPa, while the E′ values of $[sPSO_2/(PK)_{0.28}]$ and $[sPSO_2/(SiO_2)_{0.035}(PK)_{0.065}]$ are 100 and 48 MPa, respectively (data not shown). Both dry and wet $[sPSO_2/(SiO_2)_{0.035}(PK)_{0.065}]$ have a slightly higher E′ value than pristine $sPSO_2$ due to the formation of interchain hydrogen bonding cross-links between sulfonic acid, ketone, and silica hydroxyl groups. Similar cross-linking interactions were

dx.doi.org/10.1021/cm2014797 |*Chem. Mater.* 2011, 23, 4452–4458

described elsewhere[17−19,23,24] to improve the mechanical properties of hybrid Nafion-based membranes. For the wet materials, $[sPSO_2/(PK)_{0.65}]$ has a higher E′ than pristine $sPSO_2$ and $[sPSO_2/(SiO_2)_{0.035}(PK)_{0.065}]$, which is in agreement with its lower W.U.

The temperature spectra of the loss modulus (E″) and tan δ in Figure 3 reveal the presence of three thermo-mechanical relaxations for $sPSO_2$ centered at about −30, 50, and 100 °C which were ascribed to the γ, β, and α relaxations, respectively. The γ relaxation, which has the lowest energy barrier, is likely related to the local fluctuations of the aromatic rings of the $sPSO_2$ polymer chains. The β transition is associated with the relaxation modes of $sPSO_2$ side groups, which are involved in interchain dipole−dipole interactions between the sulfonic acid groups and the environment. The α relaxation is due to the segmental motion of $sPSO_2$ polymer backbone chains. The same three mechanical transitions are present for all the composite membranes. As compared to pristine $sPSO_2$, the presence of PK in the A-type materials a) shifts the α transition to higher temperatures indicating that the PK fibers reduce the mobility of the $sPSO_2$ chains and b) slightly reduces the temperature of the β and γ transitions revealing that the presence of PK decreases the strength of the interchain dipolar interactions between sulfonic acid groups, which is in agreement with the E′ values.

For the B-type membranes, the temperature of the mechanical transitions is modulated by the presence of the hybrid nanofiller due to its interactions with the $sPSO_2$ matrix. In particular, the γ transition temperature decreases with increasing hybrid nanofiller concentration. The β and α transition temperatures are changed only slightly as compared to pristine $sPSO_2$ indicating that a) the strength of the interactions between acid side groups of $sPSO_2$ and hybrid nanofiller are on the same order of those of between the $sPSO_2$ acid groups and b) the presence of $[SiO_2/(PK)_{0.65}]$ nanofiller increases the mobility of the $sPSO_2$ backbone chains as compared to that of the A-type materials. Taken together, the DMA results confirm that strength of the strong dipole−dipole interactions between acid side groups of $sPSO_2$ and the environment in the dry composite membranes decreases in the order $sPSO_2$-$sPSO_2$ > $sPSO_2$-SiO_2-PK > $sPSO_2$-PK. Furthermore, it should be highlighted that in wet samples, the $sPSO_2$-PK interchain interactions are crucial in increasing the dimensional stability and mechanical properties of membranes due to their ability to reduce the hydrophilicity of the polar side chain groups in bulk materials.

3.3. Proton Conductivity. The temperature dependence of the ionic conductivity of the wet samples is shown in Figure 4 part a) for the A-type materials and part b) for the B-type materials. The conductivity of pristine Nafion is shown as a reference.[19] It should be observed that the conductivity of the membranes increases concurrently with the water uptake values. Thus, $sPSO_2$ presents the highest values, while the A-type membranes present the lowest values. Higher conductivity values for the B-type membranes than the A-type membranes result from the presence of the $[SiO_2/(PK)_{0.65}]$ nanofiller at the interface between the hydrophobic and hydrophilic domains of the material that facilitates charge transfer between the acid groups of $sPSO_2$ and enhances the long-range charge transfer between the $sPSO_2$ acid groups due to the formation of proton percolation pathways. This effect is confirmed by analyzing the conductivities of the B-type membranes in detail. Indeed, the highest conductivity values are revealed above 75 °C for the membrane containing the highest amount of $[SiO_2/(PK)_{0.65}]$

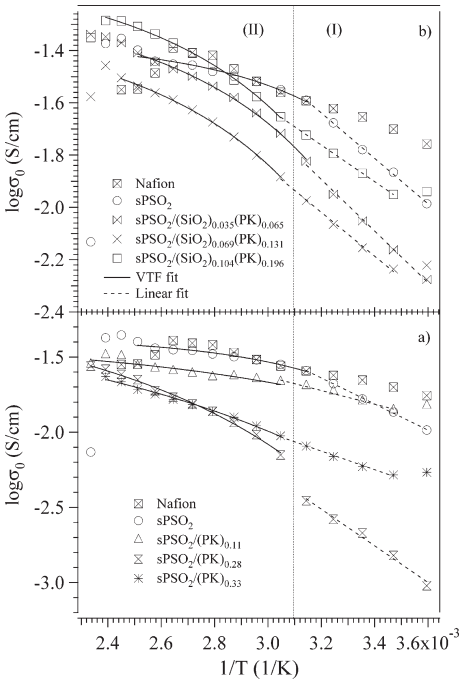

Figure 4. Plot of the bulk conductivity vs T^{-1}: a) $sPSO_2$ and A-type membranes and b) $sPSO_2$ and B-type membranes. I and II are the conductivity regions. The experimental data and the VTF and Arrhenius fit curves are indicated by markers and solid and dashed lines, respectively. σ_0 was extrapolated from the plateau of the conductivity spectra.

nanofiller. The curves in Figure 4 present two conductivity regions, I (below 50 °C) and II (above 50 °C), which are delimited by the temperature of the β mechanical relaxation event shown in Figure 3. The logarithm of σ_{dc} as a function of reciprocal temperature shows an Arrhenius dependence in region I, while in region II the typical Vogel−Tamman−Fulcher (VTF) behavior is seen.[25] Thus, the charge transfer process below 50 °C is due to proton hopping between solvated acid side groups in the A-type materials and between the solvated acid side groups and the hydroxyl groups present on the surface of silica nanoparticles in B-type materials. Above 50 °C the charge transfer process is modulated by the segmental motion of polymer chains in both A- and B-type materials. The activation energies (E_a) obtained by fitting the conductivities with Arrhenius (region I) and VTF (region II) equations[25] are reported in Table 1.

The activation energies in region I 1) decrease with increasing the hybrid nanofiller concentration for the B-type membranes, indicating that the $[SiO_2/(PK)_{0.65}]$ nanofiller enhances the long-range proton hopping process, and 2) decrease with increasing membrane storage modulus E′ for the A-type membranes (refer to part a of Figure 3) due to the presence of the PK fibers that dilute and confine the $sPSO_2$ chains. For the composite materials in region II, the E_a values are twice that of pristine $sPSO_2$ and greater for A-type materials than for B-type due to the presence of the PK fibers that, in accordance with DMA results, inhibit the $sPSO_2$ segmental motion. The congruence of the division between the conductivity regions and the DMA β transition signifies that charge transfer migration in the studied materials is directly correlated to the dynamics of the polymer host, which is significantly affected by the mechanical relaxation events of the membranes. Furthermore, in B-type membranes the pseudoactivation

dx.doi.org/10.1021/cm2014797 |Chem. Mater. 2011, 23, 4452–4458

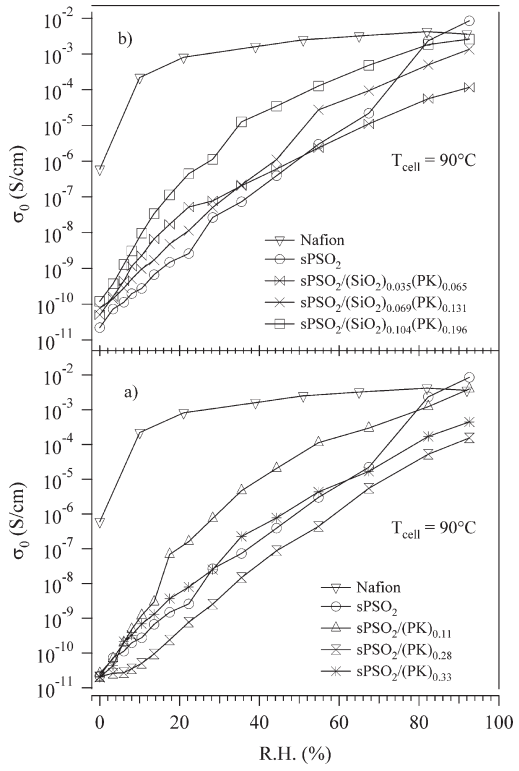

Figure 5. Plot of the bulk conductivity vs relative humidity (R.H.) at 90 °C: a) $sPSO_2$ and A-type membranes and b) $sPSO_2$ and B-type membranes. σ_0 was extrapolated from the plateau of the conductivity spectra.

energies (Table 1) are influenced only slightly by the filler-$sPSO_2$ interactions. Finally, a remarkable phenomenon occurs above 100 °C, where the conductivities of $sPSO_2$, $[sPSO_2/(SiO_2)_{0.035}(PK)_{0.065}]$, and $[sPSO_2/(SiO_2)_{0.104}(PK)_{0.196}]$ membranes are overlapped suggesting that B-type membranes are interesting materials for application in PEMFCs.

The dependence of the bulk conductivity σ_0 at 90 °C as function of the relative humidity (R.H.%) is reported in Figure 5 for the A- (part a) and B-type membranes (part b) and compared to the $sPSO_2$ reference membrane. For all samples the conductivity increases monotonically with the relative humidity toward a plateau at R.H. ≈ 100%. The effect of the hybrid nanofiller on the membranes' proton conductivity is evident for low values of relative humidity, i.e. less than 60%. In this condition, the proton conductivity of all B-type membranes is higher than that of pristine $sPSO_2$, while for A-type membranes this only occurs for the sample containing 11 wt % of PK. The hybrid nanofiller reduces the water content necessary for the long-range migration of the proton due to the formation of percolation pathways at the interfaces between the hydrophobic and hydrophilic domains present inside the material. These percolation pathways allow the B-type membranes to maintain good proton conductivity even at low water content. Furthermore, in agreement with the conductivity values measured when the materials are immersed in water (Figure 4), the highest conductivity value is obtained in the materials that exhibit the lowest β mechanical transition temperature, suggesting that the long-range conductivity in these materials occurs due to a facilitated side group relaxation, coupled with the segmental motion of the $sPSO_2$ backbone chains.

In summary, the experimental results reveal that in B-type materials the hybrid $[SiO_2/(PK)_{0.38}]$ nanofiller increases the

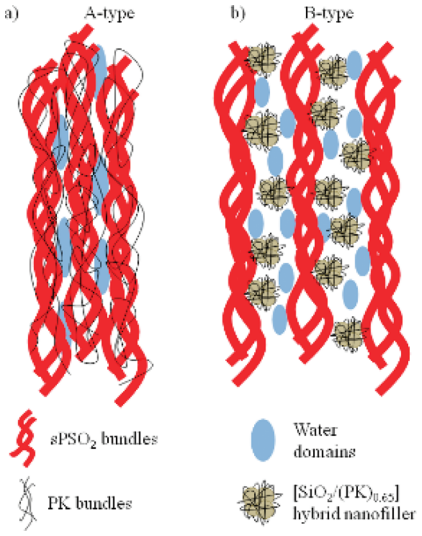

Figure 6. Schematic representation of membrane structure: a) A-type membranes and b) B-type membranes.

proton conductivity as compared to the $[sPSO_2/(PK)_x]$ membranes by maintaining strong dipolar interactions and the segmental motion of $sPSO_2$ backbone.

Recently Titvinidze et al. synthesized and studied a series of sulfonated poly(phenylene sulfone) membranes containing triphenylphosphine oxide moieties as constitutional units in the backbone, with IEC values (between 1.72 and 2.32 mequiv·g^{-1}) similar to those of the composite membranes presented here.[22] The authors reported water uptake values at 100% R.H. and room temperature between 40 and 50%, with values of λ between 19 and 28.[22] In the investigated composite membranes, despite similar values of IEC, the presence of the PK nanofibers reduces membrane swelling and water uptake due to a different membrane microstructure microstructure induced by the presence of PK nanofibers and the $[SiO_2/(PK)_{0.38}]$ nanofiller. Therefore, it is possible to hypothesize membrane structures for the A- and B-type nanocomposite membranes as reported in parts a) and b) of Figure 6, respectively.

In A-type membranes, the PK fibers, coiled around the $sPSO_2$ chains, not only reduce membrane swelling and water uptake but also reduce the proton conductivity, as compared to $sPSO_2$, by diluting the sulfonic acid groups and inhibiting the segmental motion of the $sPSO_2$ polymer chains. In B-type membranes, the hybrid nanofiller, consisting of silica nanoparticles wrapped with PK fibers, located at the interface between the hydrophobic and hydrophilic domains of $sPSO_2$ allows the material to maintain good mechanical properties and high proton conductivity values due to the formation of dipolar interactions between water, the hybrid nanofiller and the acids groups of $sPSO_2$ and due to the creation of percolation pathways at interface between the nanofiller and $sPSO_2$.

4. CONCLUSION

In this work, two series (A and B) of nanocomposite proton exchange membranes, which are based on poly(1-oxotrimethylene) (PK) and poly(*p*-phenylenesulfone) ($sPSO_2$), were prepared. A-type membranes, labeled $[sPSO_2/(PK)_x]$, consist of a blend of $sPSO_2$ containing 11, 28, and 33 wt % of PK. B-type materials consist of nanoparticles of silica covered with PK, which are

dx.doi.org/10.1021/cm2014797 |*Chem. Mater.* 2011, 23, 4452–4458

embedded in bulk poly(*p*-phenylenesulfone) material. The water uptake values of the A- and B-type membranes were half of that of pristine $sPSO_2$ and are higher for the membranes containing the hybrid nanofiller than for the $[sPSO_2/(PK)_x]$ materials. Swelling tests reveal that the presence of PK and the $[SiO_2/(PK)_{0.65}]$ nanofiller improve the mechanical stability of the composite membranes in a polar environment as compared to pristine $sPSO_2$.

Temperature dependent DMA studies conducted on dry samples showed that a) the mechanical properties, in terms of the Storage Modulus E′, of B-type materials are better than those of A-type membranes due to the presence of the hybrid nanofiller that increases the strength of the dipolar interactions between acid groups; and b) above 100 °C the E′ values for $[sPSO_2/(SiO_2)_{0.035}(PK)_{0.065}]$ and $[sPSO_2/(SiO_2)_{0.069}(PK)_{0.131}]$ are similar to those found for pristine $sPSO_2$. Furthermore, three mechanical transitions, α, β, and γ, associated with segmental motion, side group relaxation, and local fluctuation of $sPSO_2$ polymer chains were revealed, respectively, for all of the investigated materials.

Electric spectroscopy measurements performed on the fully hydrated materials and at different relative humidities reveal that the nanocomposite hybrid membranes show higher conductivity values than those of the $[sPSO_2/(PK)_x]$ membranes. Furthermore, at 90 °C and low R.H. all the membranes containing the hybrid nanofiller present conductivity values higher than those of pristine $sPSO_2$. This phenomenon is due to the presence of the inorganic nanofiller located at the interface between the hydrophobic and hydrophilic domains of the material that facilitates the charge transfer between the acid groups of $sPSO_2$ and enhances the long-range charge transfer between the $sPSO_2$ acid groups due to the formation of proton percolation pathways with high "free volumes".

Taken together, all these characteristics make B-type materials promising candidates for application in PEMFCs operating at temperatures higher than 100 °C and low humidification conditions.

AUTHOR INFORMATION

Corresponding Author

*Phone/Fax: +39 049 8275229. E-mail: vito.dinoto@unipd.it.

ACKNOWLEDGMENT

The authors thank Klaus-Dieter Kreuer for his invaluable contribution to this paper. This research was funded by the Italian Murst project PRIN2007 and NUME of FISR2003, "Sviluppo di membrane protoniche composite e di configurazioni elettrodiche innovative per celle a combustibile con elettolita polimerico".

REFERENCES

(1) Gasteiger, H. A. *Electrochemistry* **2007**, *75*, 103.
(2) Kreuer, K. D. *ChemPhysChem* **2002**, *3*, 771.
(3) Kreuer, K. D. *J. Membr. Sci.* **2001**, *185*, 29.
(4) Mauritz, K. A.; Moore, R. B. *Chem. Rev.* **2004**, *104*, 4535.
(5) Mathias, M. F.; Makharia, R.; Gasteiger, H. A.; Conley, J. J.; Fuller, T. J.; Gittleman, C. J.; Kocha, S. S.; Miller, D. P.; Mittelsteadt, C. K.; Xie, T.; Yan, S. G.; Yu, P. T. *Electrochem. Soc. Interface* **2005**, *14* (3), 24.
(6) Alberti, G.; Narducci, R.; Sganappa, M. *J. Power Sources* **2008**, *178*, 575.
(7) Harrison, W. L.; Hickner, M. A.; Kim, Y. S.; McGrath, J. E. *Fuel Cells* **2005**, *5*, 201.
(8) Alberti, G.; Casciola, M.; Massinelli, L.; Bauer, B. *J. Membr. Sci.* **2001**, *185*, 73.
(9) Kreuer, K. D. In *Handbook of Fuel Cells - Fundamentals, Technology and Applications*; Vielstich, W., Lamm, A., Gasteiger, H. A., Eds.; Wiley: Chichester, 2003; Vol. 3, p 420.
(10) Hickner, M. A.; Ghassemi, H.; Kim, Y. S.; Einsla, B. R.; McGrath, J. E. *Chem. Rev.* **2004**, *104*, 4587.
(11) de Araujo, C. C.; Kreuer, K. D.; Schuster, M.; Portale, G.; Mendil-Jakani, H.; Gebel, G.; Maier, J. *Phys. Chem. Chem. Phys.* **2009**, *11*, 3305.
(12) Schuster, M.; Kreuer, K. D.; Andersen, H. T.; Maier, J. *Macromolecules* **2007**, *40*, 598.
(13) Schuster, M.; de Araujo, C. C.; Atanasov, V.; Andersen, H. T.; Kreuer, K. D.; Maier, J. *Macromolecules* **2009**, *42*, 3129.
(14) Drent, E.; van Broekhoven, J. A. M.; Doyle, M. J. *J. Organomet. Chem.* **1991**, *417*, 235.
(15) Cavinato, G.; Toniolo, L.; Vavasori, A. *Top. Organomet. Chem.* **2006**, *18*, 125.
(16) Benetollo, F.; Bertani, R.; Bombieri, G.; Toniolo, L. *Inorg. Chim. Acta* **1995**, *233*, 5.
(17) Vittadello, M.; Negro, E.; Lavina, S.; Pace, G.; Safari, A.; Di Noto, V. *J. Phys. Chem. B* **2008**, *112*, 16590.
(18) Di Noto, V.; Piga, M.; Piga, L.; Polizzi, S.; Negro, E. *J. Power Sources* **2008**, *178*, 561.
(19) Di Noto, V.; Piga, M.; Lavina, S.; Negro, E.; Yoshida, K.; Ito, R.; Furukawa, T. *Electrochim. Acta* **2010**, *55*, 1431.
(20) Di Noto, V. *J. Phys. Chem. B* **2002**, *106*, 11139.
(21) Di Noto, V.; Lavina, S.; Wintersgill, M. C.; Fontanella, J. J. *Phys. Chem. Chem. Phys.* **2010**, *12*, 5993.
(22) Titvinidze, G.; Kaltbeitzel, A.; Manhart, A.; Meyer, W. H. *Fuel Cells* **2010**, *10* (3), 390.
(23) Di Noto, V.; Gliubizzi, R.; Negro, E.; Pace, G. *J. Phys. Chem. B* **2006**, *110*, 24972.
(24) Di Noto, V.; Gliubizzi, R.; Negro, E.; Vittadello, M.; Pace, G. *Electrochim. Acta* **2007**, *53*, 1618.
(25) Vittadello, M.; Suarez, S.; Chung, S. H.; Fujimoto, K.; Di Noto, V.; Greenbaum, S. G.; Furukawa, T. *Electrochim. Acta* **2003**, *48*, 2227.